J Mater Sci (2015) 50:2327–2336
DOI 10.1007/s10853-014-8804-0

Identification of densification mechanisms of pressure-assisted sintering: application to hot pressing and spark plasma sintering of alumina

G. Antou · P. Guyot · N. Pradeilles · M. Vandenhende · A. Maître

Received: 24 September 2014 / Accepted: 18 December 2014 / Published online: 30 December 2014

Abstract The identification of densification mechanism during hot uniaxial pressing is developed using an approach based on classical creep investigation. This approach is justified and generalised using continuum mechanics based sintering models. The benefit of this approach is to directly determine the densification parameters from the analysis of shrinkage rates of the porous material, rather than to transpose the creep mechanisms identified for dense material at given thermomechanical conditions to the densification progress. The suggested approach is applied to compare the densification mechanisms involved at the initial stage of sintering (i.e. for 60 % < relative density < 75 %) during hot pressing (HP) and spark plasma sintering (SPS) of a submicrometric alpha-alumina powder. From the stress exponent and activation energy values, it is shown that the main mechanism involves grain boundary sliding accommodated by dislocation motion and particle fracture in both cases. However, it appears that, in SPS, the high heating rate could reduce the existence of surface diffusion phenomena at the beginning of the consolidation process, as suggested by the higher activation energy compared to the one determined for HP.

Introduction

Spark plasma sintering (SPS) is a pressure-assisted sintering technique which is issued from Hot uniaxial Pressing (HP). The SPS technique allows the manufacturing of fully dense materials at lower temperatures and shorter cycle times than conventional techniques. The main difference between HP and SPS rests on the heating system: in HP, the sample is heated by a radiative furnace, whilst in SPS, the Joule effect caused by the pulsed direct current (typically a few thousand amperes and a few volts) plays directly the role of the heating source and allows high heating rates (up to 1000 °C/min). It is now well known [1] that the combination of high heating rate, dwell times of few minutes and an applied uniaxial pressure (10–100 MPa) is responsible for the enhancement of densification kinetics (i.e. sintering temperature decrease) and inhibits the microstructure evolution.

However, the whole of the physical phenomena promoted by the pulsed continuous current and the high heating rates are not fully understood. Divergent analyses of SPS mechanisms have been reported in a recent viewpoint set [2].

Different methodologies based on analytical models, such as the master sintering curve approach [3] or that suggested by Bernard-Granger and Guizard [4], have been developed in order to understand well the densification mechanisms involved during SPS. The master sintering curve approach, initially suggested for free sintering by Su and Johnson [5] and adapted for SPS by Guillon and Langer [3], assumes that the whole sintering process is governed by a unique densification mechanism. This hypothesis induces a strong limitation of this approach, and possibly identification of a densification parameter (i.e. the calculated average apparent activation energy) with no physical meaning. Additionally, densification mechanisms have been studied by using constitutive equations established for creep. Constitutive equations developed for creep (i.e. a constant volume plastic deformation process) can be

G. Antou (✉) · P. Guyot · N. Pradeilles · M. Vandenhende · A. Maître
Laboratoire Sciences des Procédés Céramiques et Traitements de Surface, UMR CNRS 7315, Centre Européen de la Céramique, 12, rue Atlantis, 87068 Limoges Cedex, France
e-mail: guy.antou@unilim.fr

used for densification (i.e. a volume change process) when the strains due to densification and creep are separated, as suggested by Raj [6]. Consequently, as recently reminded by Chakravarty and Chokshi [7], during HP and SPS in contrast to sinter forging, the ratio between the densification and creep strains is fixed and equal to 2/3 due to the axial constraints from the die ($\varepsilon_{xx} = \varepsilon_{yy} = 0$), thereby enabling the use of the standard creep equation for evaluating densification kinetics. This transposition also assumes that the main driving force of pressure-assisted sintering is due to the macroscopic applied pressure by neglecting the contributions from pressure-less sintering [8] and, in the case of SPS, specific effects that can occur such as electromigration [9], electromagnetic effect [10] or thermal diffusion involved by possible high local temperature gradients [11]. Such an approach developed by Bernard-Granger and Guizard [4] has been widely applied in literature to several ceramic systems [4, 12–15]. Densification mechanisms were studied and comparison between HP and SPS were conducted in order to highlight potential discrepancies between SPS versus HP. In a recent paper [16], we show that, even if this approach is attractive by the low amount of experiments to elucidate the densification mechanism, the identified densification parameters can be potentially biased. The main reason is the strong dependence of the determined densification parameters to precise evaluations of the effective stress acting on the powder bed and of the effective shear modulus.

In this work, we use a robust approach to identify sintering mechanisms for which the effective stress acting on the powder bed is not required. This investigation consists in analysing shrinkage kinetics evolution under isothermal and isobar conditions at invariant microstructure. This approach which leads to reliable densification parameters is justified by continuum micromechanical models that integrate the whole stress field. It is applied to compare the densification mechanisms involved at the early stages of sintering during HP and SPS of an alumina powder used as an electrically non-conductive model material. The objective is to bring out possible discrepancies in plastic deformation mechanisms that can be related to specific thermal effects induced during SPS.

Constitutive models for HP

Transposition of constitutive model for HIP

Models by diffusional mass transport under the driving forces of surface curvature and applied stress were initially formulated by Coble for hot isostatic pressing (HIP) [17]. HIP is viewed in a manner analogous to that of creep in dense solids, and the creep equations were modified to account for the porosity and the surface curvature appropriate to porous powder systems. When the applied stress is much greater than the driving force due to surface curvature, the densification rate in HIP can be expressed generally as follows [18]:

$$\frac{1}{\rho}\frac{\mathrm{d}\rho}{\mathrm{d}t} = \frac{HD\varphi^n}{d^p kT}\sigma_{\mathrm{a}}^n, \tag{1}$$

where ρ is the relative density, H is a numerical constant, ϕ is the stress intensification factor that describes how the macroscopic isostatic applied stress (σ_a) is magnified at the microscopic scale, d is the grain size, k is the Boltzmann constant, T is the absolute temperature, the grain size and stress exponents p and n depend on the mechanism of densification.

$$D = D_0 \exp\left(-Q/RT\right) \tag{2}$$

is the diffusion coefficient of the rate-controlling species with Q the associated apparent activation energy, D_0 a pre-exponential coefficient and R = 8.314 J mol^{-1} K^{-1}.

This model well-adapted for HIP process does not take into account the whole stress field acting on the powder bed in the case of HP process. As a matter of fact, the radial and tangential stresses, which are related to the axial constraints from the die and can be thermally generated by radial thermal gradients and thermal expansion mismatch between the powder and the die, are not considered [19]. Consequently, during the anisothermal stage in HP configuration, this model is only valid when the coefficient of thermal expansion of the powder is significantly lower than that of the graphite die. During the isothermal stage, the thermal stresses are reduced due to the plastic deformation (or creep) of materials.

In the following, the theory of nonlinear-viscous flow of porous solids that integrates the whole stress field acting on the powder bed is described.

Model of nonlinear-viscous flow of porous solids

Based on the theory of plasticity for porous metals and metal powders [20, 21], continuum mechanics based sintering models have been developed and considered an elliptic equivalent effective stress acting on the powder bed which is a combination of the deviatoric and hydrostatic parts of the stress field:

$$\sigma_{\mathrm{eq}}^2 = c(\rho)\sigma_{\mathrm{e}}^2 + f(\rho)\sigma_{kk}^2, \tag{3}$$

where the constants c and f depend on the relative density, the von Mises equivalent stress being $\sigma_{\mathrm{e}} = \sqrt{(3/2)\sigma_{ij}'\sigma_{ij}'}$ and the deviatoric stress $\sigma_{ij}' = \sigma_{ij} - \sigma_{kk/3}$. When $\rho = 1$ (dense material), $f = 0$ and c = 1, and the elliptic equivalent effective stress reduces to the von Mises equivalent stress. This criterion is hence an extension of the von Mises criterion to porous material. The density-related terms f and

c can have various mathematical expressions owing to different approaches in the literature [22–24].

Abouaf and Chenot [22] showed within a thermodynamical frame that deformation rate can be written from the equivalent effective stress and viscoplastic potential (Ω) through

$$\dot{\varepsilon}_{ij} = \frac{1}{\sigma_{eq}} \frac{\partial \Omega}{\partial \sigma_{eq}} \left(\frac{3}{2} c(\rho) \sigma'_{ij} + f(\rho) \sigma_{kk} \delta_{ij} \right). \quad (4)$$

Assuming that the viscoplastic work of the matrix material is the same as that of the porous material, the creep strain rate can be written as

$$\dot{\varepsilon}_{ij} = \frac{\rho \dot{\varepsilon}_{eff}}{\sigma_{eq}} \left(\frac{3}{2} c(\rho) \sigma'_{ij} + f(\rho) \sigma_{kk} \delta_{ij} \right), \quad (5)$$

where $\dot{\varepsilon}_{eff} = \frac{\dot{\varepsilon}_0 \sigma_{eq}^n}{d^p kT} \exp(-Q/RT)$ corresponds to the Mukherjee-Bird-Dorn creep equation for dense material [25] characterised by a numerical constant ($\dot{\varepsilon}_0$) and internal parameters such as the apparent activation energy (Q), the grain size exponent (p) and the stress exponent (n). In a HP process, considering the axial constraints from the die along the z axis, the previous relation simplifies as

$$\dot{\varepsilon}_{zz} = -\frac{1}{\rho} \frac{d\rho}{dt} = \dot{\varepsilon}_0 \rho \left(\frac{9 f(\rho) c(\rho)}{c(\rho) + 4 f(\rho)} \right)^{\frac{n+1}{2}} \frac{(\sigma_{zz})^n}{d^p kT} \exp(-Q/RT). \quad (6)$$

As noted by Besson and Abouaf [26], it is interesting to point out that this model is equivalent to the models proposed by Scherer [27] and Bordia [28] when the material has a linear creep law. When the material is nonlinear, there is an interaction between shear and pressure which implies that for a given pressure an additional shear stress enhances the densification.

The general model of Abouaf and Chenot [22], which describes the main stages of the sintering (creation of necks between powder particles and removing of the open and isolated porosities) through a unique model, is widely used in the literature for consolidation study by finite element method. It can be noticed that this model is in good agreement with HP/SPS experimental data [24, 29].

Similarly, based upon the initial works of Skorohod [30], Olevsky [31] has developed the following constitutive relationship to describe the creep stress in a nonlinear-viscous porous material by considering an effective strain rate instead of an effective stress:

$$\sigma_{ij} = \frac{\sigma_0(W)}{W} \left(\phi(\rho) \dot{\varepsilon}_{ij} + \psi(\rho) \dot{e} \delta_{ij} \right), \quad (7)$$

where the normalised shear modulus $\varphi(\rho)$ and the normalised bulk viscosity modulus $\Psi(\rho)$ are porosity functions, and W is the effective strain rate of porous material.

$$W = \frac{1}{\sqrt{\rho}} \sqrt{\psi(\rho) \dot{e}^2 + \phi(\rho) \dot{\gamma}^2}, \quad (8)$$

where $\dot{e}$ and $\dot{\gamma}$ are invariants of the strain rate tensor $\dot{\varepsilon}_{ij}$.

For pressing in a rigid die, $\dot{e} = \dot{\varepsilon}_{zz}, \dot{\gamma} = \sqrt{2/3}|\dot{e}|$, $\dot{\varepsilon}_{zz}$ is the axial strain rate. Hence, considering the Mukherjee-Bird-Dorn equation [25] for the creep of dense material (σ_0 (W)), Eq. (7) reduces to [32]

$$\dot{\varepsilon}_{zz} = -\dot{\varepsilon}_0 \left(\sqrt{\frac{\rho}{\frac{2}{3}\phi(\rho) + \psi(\rho)}} \right)^{1+\frac{n}{2}} \frac{(\sigma_{zz})^n}{d^p kT} \exp(-Q/RT). \quad (9)$$

As previously shown, models for nonlinear-viscous flow of porous solids reduce to kinetic equations [Eqs. (6) and (9)] similar to Eq. (1) for the normalised shrinkage rate in the case of pressing in a rigid die.

The approach used to identify reliable densification parameters

The approach based on classical creep investigation, that consists in comparing the normalised shrinkage rates under isothermal and isobar conditions at given relative density for several grain sizes, allows identifying the key parameters of densification mechanism (i.e. stress and grain size exponents, and apparent activation energy). This approach has been initially suggested based on constitutive model for configuration of isostatic stress field, i.e. in HIP setup [7, 18, 33]. It can be used in HP setup by assuming that, during the isothermal stage, the thermally generated stresses are negligible due to the plastic deformation (or creep) of materials and do not affect the identification of densification parameters. As reminded in the previous section, this approach can be generalised, since continuum mechanics based sintering models suggest that the effective stress, which is a combination of the hydrostatic and deviatoric parts of the stress field, depends only on the relative density. Consequently, constitutive sintering models effectively simplify to an equation similar to HIP Eq. (1) in the case of pressing in a rigid die.

Moreover, the benefit of this approach, compared to previous works of [24, 26, 34, 35] which consider the transposition of the creep mechanisms identified for dense material under given thermomechanical conditions to their porous state, is to directly determine the densification parameters from analysis of shrinkage rates of the porous material. In previous works, the effect of density is integrated via an effective stress evaluated from the macroscopic applied stress by considering a stress intensity factor. However, it assumes that the deformation mechanisms of grains are not affected by the presence of unconstrained surfaces of the grains related to inter-

granular pores during the initial and intermediate sintering stages (i.e. for $\rho < 90$ %). This assumption is not obvious, since, as reminded by Rahaman [18], the atomic flux field and the path length for diffusion can be affected by the porous state. In the creep of dense solids, the atomic flux terminates at the boundaries under tension, whereas in hot pressing, the flux terminates at the pore surfaces. The grain boundary area, which is related to the grain size, remains constant during creep, but both the grain boundary area and the path length for diffusion increase during hot pressing. The present approach allows highlighting involved mechanisms, not only dependent on effective stress-temperature-grain size for a given material, but which can also be altered by the porous state.

Application to the HP and SPS sintering of an alumina powder

In the literature, there have been few studies that examined alumina densification mechanisms involved during pressure-assisted sintering such as HP and SPS. Several authors [12–14, 36] applied the biased approach suggested by Bernard-Granger et al. [4] leading to a wide discrepancy in the calculated densification parameters, i.e. stress exponent and activation energy ranging between 1 and 4 and from 150 to 644 kJ mol^{-1}, respectively. Hence, following this approach, no sole SPS mechanism has been identified for the intermediate and final sintering stages. Only two recent works [7, 33] have been conducted on alumina following the suggested creep approach to identify reliable densification parameters. Langer et al. [33] applied this approach to compare the densification behaviour of submicrometric (i.e. mean grain sizes of 150 and 500 nm) alumina powders sintered by HP and SPS with temperatures ranging from 1100 to 1200 °C and applied stresses from 15 to 50 MPa. For the considered intermediate sintering stage (i.e. 75 % $< \rho <$ 85 %), the authors reveal similar densification parameters ($n \sim 1$, $m \sim 3$, Q_d around 420–430 kJ mol^{-1}) for HP and SPS, probably linked to the very low heating rate used in SPS (i.e. 10 °C min^{-1}). Recently, similar creep process of grain boundary diffusion was identified by Chakravarty and Chokshi [7] for the intermediate and final stages of sintering (i.e. respective densities of 75 and 93 %) during SPS experiments (with temperatures ranging from 900 to 1150 °C and applied stresses from 25 to 100 MPa) of similar high purity alumina of nominal particle size of 100 nm.

In this work, we focus on the initial stage of sintering (i.e. $\rho < 75$ %), since the major benefits of SPS process are claimed to be involved at the beginning of the consolidation process. The objective is to study the potential discrepancy between HP and SPS, and to analyse the involved deformation mechanisms.

In order to apply the suggested approach for the identification of densification parameters, the densification kinetic data obtained in a previous work [16] are considered and additional sintering experiments are conducted. The experimental conditions are summarised below.

Experimental procedure

The experiments were performed both on a Hot Pressing device, model Goliath Graphite 2000, provided by La Physique Appliquée, located at the S.P.C.T.S. in Limoges, and a SPS device, model Dr. Sinter 2080, provided by Fuji Electronics Industrial Co. Ltd., Japan, located at the Plateforme Nationale de Frittage Flash (PNF^2) in Toulouse. The powder used is an α-alumina powder, 99.99 % pure, with a median particles size of 140 nm (TM-DAR, TaiMei Chemicals, Japan).

For both experiments, 2.5 g of powder was poured into a graphite die with an inner diameter of 20.4 mm. A compressible graphite foil (0.2 mm thick, Papyex®, Mersen, France) was used as lubricant to coat the inner surface of the die and the surface of the punches. Identical die geometry was used in both cases to compare the results obtained on HP and SPS devices.

In the HP, the temperature of the sample is measured by a thermocouple placed near the die. This thermocouple has been calibrated to give similar temperature than that previously recorded by a thermocouple placed at the centre of the die, in order to know the real temperature in the sample core. In the SPS, the temperature is measured by a pyrometer focused on the die. Experiments have been formerly conducted to quantify the discrepancy between the temperature of the sample and the temperature of the surface of the die. The temperatures measured by the pyrometer were averagely underestimated by 60 °C on the dwell, according to calibration tests.

On the HP device, tests were performed at different temperatures (900, 950 and 1000 °C), under an applied stress of 20, 35, 42.5 and 50 MPa. The heating rate was 15 °C min^{-1}, and the dwell time was 60 min. On the SPS device, tests were performed at similar temperatures (1010, 1060 and 1110 °C), under an applied stress of 35, 42.5 and 50 MPa. The heating rate was 100 °C min^{-1}, and the dwell time was 15 min. Sintering parameters were optimised to focus the study of densification kinetics on the same density range corresponding to the initial stage of sintering, even if temperatures for HP and SPS devices are slightly different.

In both cases, the displacement was recorded by the device, and for each experiment, a blank cycle was performed by submitting a fully dense pellet to a complete heating cycle, in order to remove the dilatation of the die, punches and alumina from the recorded data.

Structural and morphological observations were carried out by transmission electron microscopy (TEM). The study was performed using a high-resolution Jeol JEM-2100F microscope (Jeol Ltd., Tokyo, Japan). The thin foils for TEM were prepared by cutting thin slices with diamond wire (2×2 mm^2 section). These slices were then ground, dimpled and finally thinned down to perforation by Ar-milling with a 4 kV accelerating voltage with PIPS 691 apparatus (GATAN Inc., Pleasanton, USA).

Results

The evolution of the relative density on the isothermal dwell was calculated from the recorded axial displacement via the following expression:

$$\rho_i = \rho_f . \frac{h_f}{h_i}, \tag{10}$$

where ρ_i is the instantaneous relative density, ρ_f the final relative density (measured by Archimedes method and geometrically), h_f the final height of the sample and h_i the instantaneous height of the sample.

To identify the densification parameters (i.e. stress exponent and apparent activation energy values) by the suggested approach, shrinkage rates are compared in isothermal and isobar conditions for identical microstructures, i.e. for the same density and without the occurrence of grain growth as shown in Fig. 1a, b for the selected limit sintering conditions.

Moreover, it is also important to compare the shrinkage rates calculated at the same sintering state. It is possible to separate the shrinkage into two main areas, as shown in Fig. 2: (i) a first one, at a lower density, during which the shrinkage rate decreases dramatically, and (ii) a second one, at a higher density, during which the shrinkage rate decreases more slowly. For a given material, the threshold density separating these two typical stages depends on the temperature and at a lesser degree on the applied stress. The first stage may be related to the accommodation of the effective stress, followed by a slower microstructural modification corresponding to a better stress distribution inducing lower shrinkage rates. The comparison of the shrinkage rates only makes sense if the chosen density belongs to the same area for each test.

Stress exponent

In order to determine the stress exponent, it is necessary to perform several tests using the same heating cycle, and compare the shrinkage rates at the same density, but for different applied stresses. During the isothermal dwell, the stress exponent values are determined from the slope of the curve representing $\ln\left(\frac{1}{\rho}\frac{d\rho}{dt}\right)$ as a function of $\ln(\sigma_{zz})$ (Fig. 3). Although the imposed ranges of thermomechanical conditions are restricted (i.e. variations of temperature of 50 °C and of applied stress of 7.5 MPa), the overlapping of density ranges is restricted, and the identification of kinetics data at fixed densities belonging to the initial stage of sintering is limited. This is an intrinsic limitation of this approach for this low density range.

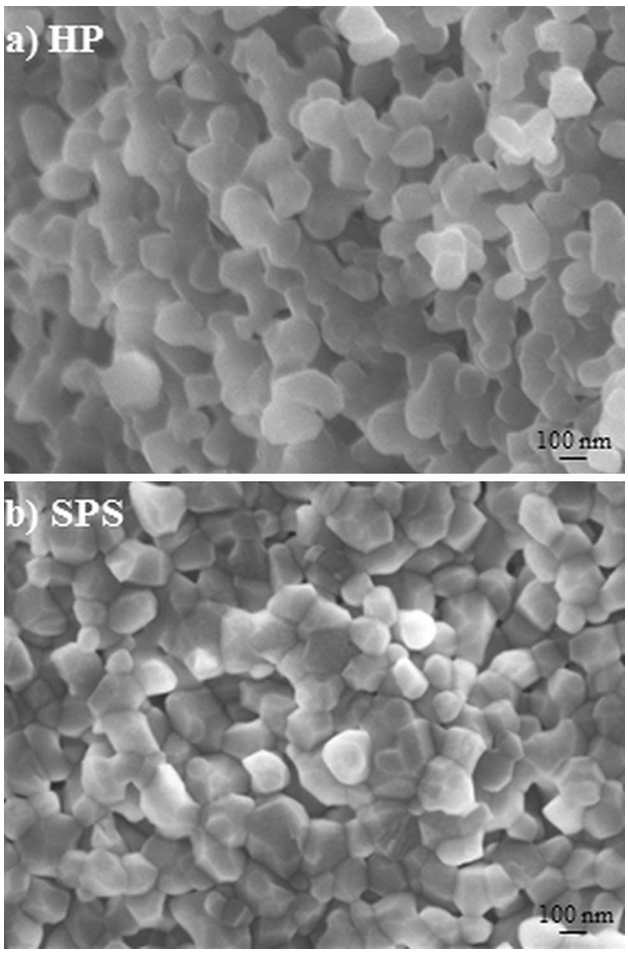

Fig. 1 Typical overview by field emission gun scanning electron microscopy observations of the samples: **a** HP sintered at 1000 °C under 50 MPa (final relative density of 87 %); **b** SPS sintered at 1110 °C under 50 MPa (final relative density of 81 %)

One can notice that the stress exponent values are rather high for both HP and SPS. It varies between 2.0 and 3.1 in HP and between 2.3 and 2.7 in SPS. This means the deformation rate is strongly affected by the applied stress, in the temperature, stress and relative density ranges which were studied.

The stress exponent values which were found to exclude the possibility of a densification mechanism driven by grain boundary ionic diffusion ($n = 1$), as mostly found in the literature at higher density (i.e. >75 %) for pure α-alumina of similar grain size around 100 nm [7, 32]. A value of 2 can

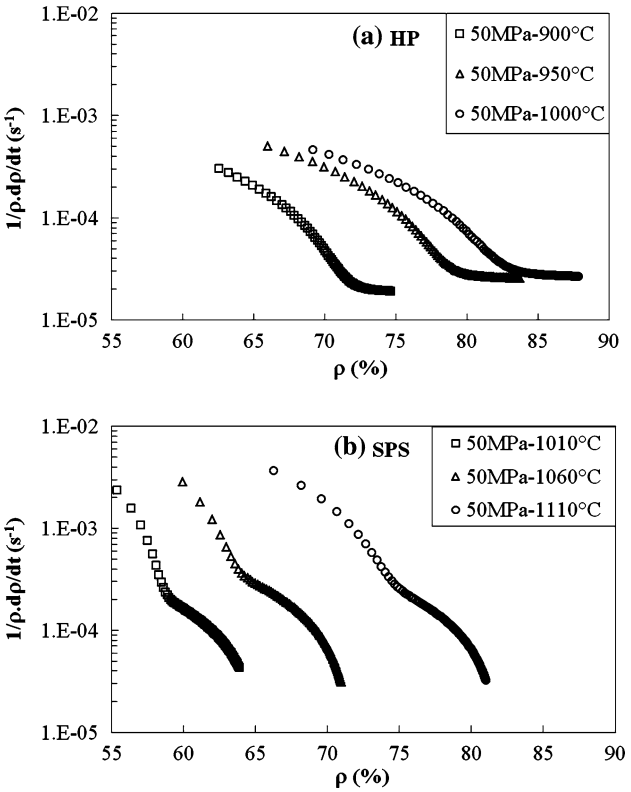

Fig. 2 Typical evolution of the normalised shrinkage rates as a function of the density during the isothermal dwell in isobar modes for **a** HP (applied stress of 50 MPa and dwell temperatures ranging from 900 to 1000 °C) and **b** SPS (applied stress of 50 MPa and dwell temperatures ranging from 1010 to 1110 °C)

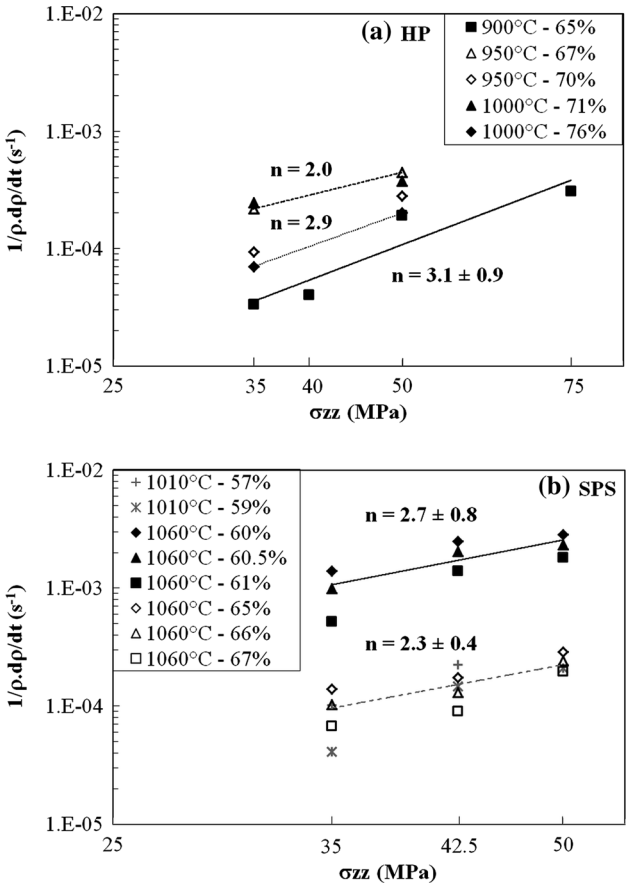

Fig. 3 Stress exponent values determined for **a** HP and **b** SPS

imply grain boundary sliding (GBS) or interface-controlled diffusion mechanisms, whilst a value of 3 or more can imply dislocation creep. These hypotheses will be discussed along with microstructural observations in §4.3.

Apparent activation energy

As shown by Eqs. (6) and (9), the apparent activation energy can be evaluated for a given applied stress and a given relative density by calculating the slope of the line representing $\ln\left(\frac{1}{\rho}\frac{\mathrm{d}\rho}{\mathrm{d}t}\right)$ as a function of $-\frac{1}{RT}$ (Fig. 4). The calculated apparent activation energy is higher in SPS. These energies and the involved densification mechanisms will be discussed in the next section.

TEM observations and discussion

During the considered initial stage of pressure-assisted sintering, not only plastic deformation and creep of particles, but also their rearrangement and fractioning can take place. Consequently, in the following, additionally to the determined densification parameters (i.e. stress exponents and activation energies) that reflect the macroscopic thermomechanical behaviour of the porous solid, the involved densification mechanisms will be discussed based on high-resolution TEM structural observations performed on the sintered samples.

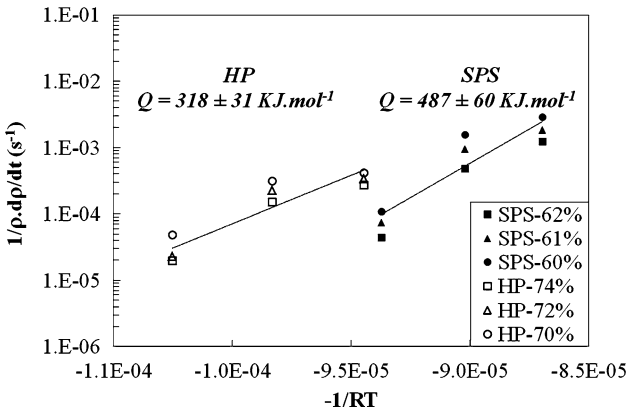

Fig. 4 Calculated apparent activation energies for HP (applied stress of 50 MPa and dwell temperatures of 900–950–1000 °C) and SPS (applied stress of 42.5 MPa and dwell temperatures of 1010–1060–1110 °C)

The existence of dislocations is clearly evidenced in HP and SPS specimens, as shown in Fig. 5a, b through diffraction contrasts within some particles. These contrasts arise from coherent elastic scattering of electrons at special Bragg angles and are related to dislocations within particles that cause local distortions of the surrounding crystal. Thus, even if the rhombohedral primitive cell structure of α-alumina has very few sliding plans available to lead to dislocation mobility [37], it appears that the plastic deformation of alumina particles involves dislocation motion for the applied thermomechanical conditions.

These observations and the measured stress exponent values agree with the work of Ruano et al. [38] that reviewed creep data from over 40 different polycrystalline alumina materials and concluded that the dominant deformation mechanism in creep of fine-grained alumina is GBS accommodated by dislocation motion.

Moreover, an important amount of fractured particles have been observed, most of them having one of their dimensions over 100 nm (Fig. 6a, b, c, d). This phenomenon can be compared to the one recently observed by Calvié et al. [39] on δ-alumina, showing the existence of a limit between ductility and fragility depending on the grain size. The authors showed that above a given dimension (between 40 and 120 nm), δ-alumina becomes fragile, and due to its geometry, they foresee a lower threshold for α-alumina. Having a 140 nm mean diameter, TM-DAR alumina seems to be in the fragility range, which justifies the observation of fractured particles. Moreover, for the considered low densities around 60–70 %, it is possible to evaluate the effective stress acting on the particles using Helle's geometrical model obtained for HIP conditions [34], which leads to an under-estimation by neglecting the thermally generated radial and tangential stresses. The estimated effective stress continuously decreases whilst the density rises, starting around 700 MPa. According to Wachtman et al. [40], these values of several megapascals are above the strength of sapphire which depends on the solicitation direction compared to the sliding plane and decreases with temperature up to 800 °C. Moreover, Alvarez-Clemares et al. [41] have recently shown, by HR-TEM characterisation, the presence of intra-granular cracks in dense pellets of TM-DAR alumina sintered by SPS (macroscopic applied stress of 80 MPa, heating rate of 50 °C min^{-1} and dwell of 2 min at 1300 °C). So the effective stress seems to be high enough to lead to particle fracture.

Consequently, it seems that, for the considered initial sintering stage of submicrometric alumina powder, densification mechanism is related to GBS accommodated by dislocation motion and particle fracture. As a matter of fact, GBS becomes blocked or inhibited from further sliding at regions such as triple points or grain boundary ledges. These impediments can be removed by dislocation motion or by particle fracture. This last phenomenon not encountered during creep of dense alumina ceramics can be favoured by the porous state during sintering due to the presence of unconstrained surfaces of grains related to inter-granular pores.

For higher densities, as the local effective stress decreases due to a more homogeneous distribution of the applied macroscopic stress, the dominant densification mechanism changes from plastic flow caused by GBS at initial sintering stage to diffusion creep at intermediate and final sintering stages as shown by [7, 33]. Similar densification mechanism evolution has been observed by Morita et al. [42] for fine-grained $MgAl_2O_4$ spinel sintered by SPS: change from partial dislocation motion to diffusion creep has been observed by TEM as the density increases.

Considering the determined apparent activation energies, the determined values for HP and SPS are very dissimilar, respectively, of 318 ± 31 and 487 ± 60 kJ mol^{-1}. The low value for HP is close to the activation energy around 230–280 kJ mol^{-1} associated to surface diffusion [18]. Micrometric agglomerates in the initial powder (detected by granulometry and BET measurements) would undergo surface diffusion phenomena that lead to local densification during the initial stage of HP sintering. Raether et al. [43]

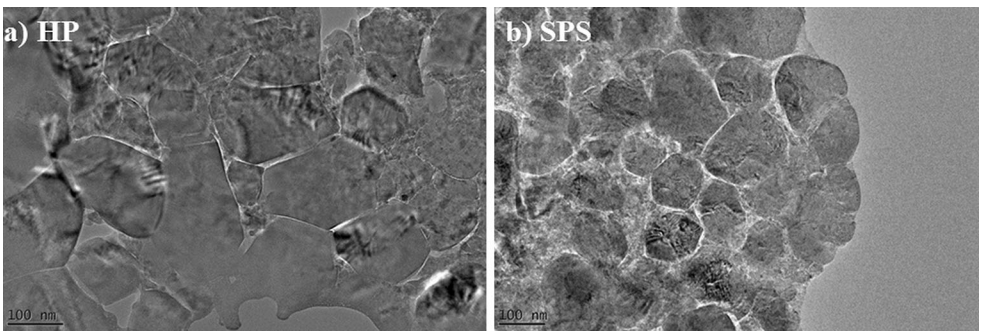

Fig. 5 Typical overview by TEM structural observations of the samples: **a** HP sintered at 950 °C under 35 MPa (final relative density of 78 %); **b** SPS sintered at 1110 °C under 35 MPa (final relative density of 75 %)

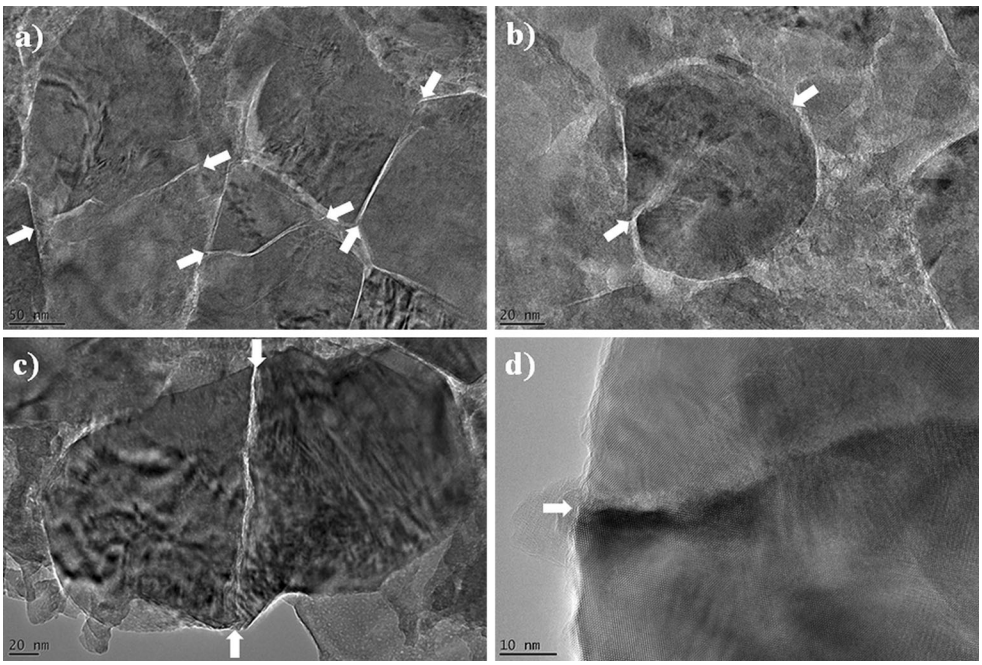

Fig. 6 TEM observations at several magnifications of a sintered alumina sample (HP, 950 °C, 35 MPa, relative density: 78 %) showing fractured particles. The *white arrows* point the corresponding fractures

have observed the increase of the apparent activation energy from 250 to 496 kJ mol^{-1} during densification of TM-DAR alumina powder sintered by free sintering and sinter forging with heating rates from 5 to 20 °C min^{-1} and dwell temperatures ranging from 890 to 1000 °C, similar to the present HP conditions. They discussed these low activation energies at the beginning of consolidation based on microscope observations of quenched samples at several densities, and hence they show the preferential sintering within agglomerates by the elimination of small intra-agglomerate pores.

On the opposite, during SPS, as suggested by Brook [44], a high heating rate would increase shrinkage kinetics and allow leaving faster the temperature range for which surface diffusion is dominant and avoiding too early intergranular pore spheroidization [3]. The difference of activation energies between HP and SPS during the initial sintering stage (i.e. for 60 % $< \rho <$ 75 %) would be related to a superior heating rate in SPS, which reduces surface diffusion regime. For higher temperatures between 1100 and 1200 °C and higher densities ranging from 75 to 85 %, Langer et al. [33] found similar grain boundary diffusion mechanism both in HP and SPS.

Finally, for the considered temperature range (i.e. 900–1100 °C), discrepancy exists between HP and SPS treatments in isothermal conditions at the initial stage of sintering (i.e. for 60 % $< \rho <$ 75 %). On one hand, from the determined stress exponents and activation energies, a densification mechanism involving GBS accommodated by dislocation motion and particle fracture is proposed in the case of HP. On the other hand, for SPS, similar mechanism is identified, but the higher apparent activation energy is close to that measured during creep experiments of dense alumina around 475 kJ mol^{-1} [41] that is attributed to ionic grain boundary diffusion. However, as shown by the review of Heuer on major diffusion processes in α-Al_2O_3 [45], it is difficult to state about the involved species diffusion.

These results are in good agreement with the fast firing concept put forward by Brook [44]. As a matter of fact, when a material such as alumina exhibits activation energy for densification higher than that for coarsening, the ratio of the densification rate to the coarsening rate is larger at higher temperatures. The faster the sample is heated through the low-temperature region, where the ratio of densification rate to coarsening rate is unfavourable, the higher the density with fine-grained microstructure. Zhou et al. [46] demonstrated heating rate benefits to full densification with reduced grain growth in submicrometric alumina sintered by SPS. It was found that the grain growth rate decreased with increasing heating rate.

Conclusions

In this work, the generalisation of an approach based on classical creep investigation used to identify the key parameters of densification mechanism (i.e. stress and

grain size exponents, and apparent activation energy) has been justified using continuum mechanics based sintering models. This approach consists in comparing the normalised shrinkage rates in isothermal and isobar conditions at given density for several grain sizes.

The benefit of this approach, compared to previous works of [24, 26, 34, 35] which consider the transposition of the creep mechanisms identified for dense material at given thermomechanical conditions to their porous state, is to directly determine the densification parameters from analysis of shrinkage rates of the porous material. Consequently, it allows highlighting involved deformation mechanisms of grains, not only dependent on temperature-stress-grain size for a given material, but which can also be altered by the porous state, and in particular by the presence of unconstrained surfaces of the grains related to inter-granular pores during the initial and intermediate sintering stages (i.e. for $\rho < 90$ %).

The suggested approach has been applied to compare the densification mechanisms involved at the initial stage of sintering (i.e. for 60 % $< \rho <$ 75 %) during HP and SPS of a submicrometric alumina powder. It has been shown that the main mechanism involved GBS accommodated by dislocation motion and particle fracture in both cases. However, it seemed that, in SPS, the high heating rate, that is a thermal effect, could reduce the existence of surface diffusion phenomena at the beginning of the consolidation process, as suggested by the higher activation energy compared to the one determined for HP.

The application of this approach to materials exhibiting good electrical conductivities should allow studying non-thermal effects of the electrical current on densification mechanisms.

Acknowledgements This work was carried out within the IMPULSE project, thanks to the financial support of the French National Research Agency (ANR). The authors gratefully thank the group of Dr Claude ESTOURNES (CIRIMAT Institute) and the PNF^2 team for their help in carrying out SPS experiments.

References

1. Munir ZA, Anselmi-Tamburini U, Ohyanagi M (2006) The effect of electric field and pressure on the synthesis and consolidation of materials: a review of the spark plasma sintering method. J Mater Sci 41(3):763–777
2. Risbud SH, Han Y-H (2013) VP Set 54 Editors, preface and historical perspective on spark plasma sintering. Scr Mater 69(2):105–206
3. Guillon O, Langer J (2010) Master sintering curve applied to the field-assisted sintering technique. J Mater Sci 45:5191–5195
4. Bernard-Granger G, Guizard C (2007) Spark plasma sintering of a commercially available granulated zirconia powder: I. Sintering path and hypothesis about the mechanism(s) controlling densification. Acta Mater 55:3493–3504
5. Su H, Johnson DL (1996) Master sintering curve: a practical approach to sintering. J Am Ceram Soc 79(12):3211–3224
6. Raj R (1982) Separation of cavitation-strain and creep-strain during deformation. J Am Ceram Soc 65(3):C-46
7. Chakravarty D, Chokshi A (2014) Direct characterizing of densification mechanisms during spark plasma sintering. J Am Ceram Soc 97(3):765–771
8. Bordia RK, Raj R (1988) Sintering of TiO_2-Al_2O_3 composites: a model experimental investigation. J Am Ceram Soc 71(4):302–310
9. Olevsky EA, Froyen L (2006) Constitutive modeling of spark-plasma sintering of conductive materials. Scr Mater 55:1175–1178
10. Guyot P, Rat V, Coudert JF, Jay F, Maître A, Pradeilles N (2012) Does the Branly effect occur in spark plasma sintering? J Phys D Appl Phys 45(9):92001–92004
11. Olevsky EA, Froyen L (2009) Impact of thermal diffusion on densification during SPS. J Am Ceram Soc 92(S1):S122–S132
12. Bernard-Granger G, Guizard C (2009) Densification mechanism involved during spark plasma sintering of a codoped α-alumina material: Part I. Formal sintering analysis. J Mater Res 24(1):179–186
13. Gurt-Santanach J, Weibel A, Estournès C, Yang Q, Laurent C, Peigney A (2011) Spark plasma sintering of alumina : study of parameters, formal sintering analysis and hypotheses on the mechanism(s) involved in densification and grain growth. Acta Mater 59(4):1400–1408
14. Demuynck M, Erauw JP, Van der Biest O, Delannay F, Cambier F (2012) Densification of alumina by SPS and HP: A Comparative Study. J Europ Ceram Soc 32:1957–1964
15. Gendre M, Maitre A, Trolliard G (2010) A study of the densification mechanisms during spark plasma sintering of zirconium (oxy-)carbide powders. Acta Mater 58:2598–2609
16. Guyot P, Antou G, Pradeilles N, Weibel A, Vandenhende M, Chevallier G, Peigney A, Estournès C, Maître A (2014) Hot pressing and spark plasma sintering of alumina: discussion about an analytical modelling used for sintering mechanism determination. Scr Mater 84–85:35–38
17. Coble RL (1970) Diffusion models for hot pressing with surface energy and pressure effects as driving forces. J Appl Phys 41:4798–4807
18. Rahaman MN (2008) Sintering of Ceramics. CRC Press, Tayor & Francis Group, New York, pp 81–97
19. Antou G, Gendre M, Trolliard G, Maître A (2009) Spark plasma sintering of zirconium carbide and oxycarbide: finite element modeling of current density, temperature, and stress distributions. J Mater Sci 24(2):404–412
20. Kuhn HA, Downey CL (1971) Deformation characteristics and plasticity theory of sintered powder materials. Int J Powder Metall 7:15–25
21. Green R (1972) A plasticity theory for porous solids. Int J Powder Metall 14:215–224
22. Abouaf M, Chenot J (1986) A numerical model for hot deformation of metal powders. J Theor Appl Mech 5:121–140
23. Cocks AC (1989) Inelastic deformation of porous materials. J Mech Phys Solids 37(6):693–715
24. Wolff C, Mercier S, Couque H, Molinari A (2012) Modeling of conventional hot compaction and spark plasma sintering based on modified micromechanical models of porous materials. Mech Mater 49:72–91
25. Mukherjee A, Bird J, Dorn J (1969) Experimental correlation for high-temperature creep. Trans ASM 62:155–179
26. Besson J, Abouaf M (1992) Rheological of porous alumina and simulation of hot isostatic pressing. J Am Ceram Soc 75(8):2165–2172

27. Scherer GW (1979) Sintering inhomogeneous glasses: application to optical waveguides. J Non-Cryst Solids 34:239–256
28. Bordia RK, Scherer GW (1988) On constrained sintering—I. Constitutive model for a sintering body. Acta Metall 36(9):2393–2397
29. Cho JH, Kim KT (2001) Densification of mixed metal powder at high temperature. Int J Mech Sci 43:921–933
30. Skorohod VV (1972) Rheological basis of the theory of sintering. Naukova Dumka, Kiev
31. Olevsky EA (1998) Theory of sintering: from discrete to continuum. Mat Sci Eng R23:41–100
32. Olevsky EA, Bogachev I, Maximenko A (2013) Spark-plasma sintering efficiency control by inter-particle contact area growth: a viewpoint. Scr Mater 69:112–116
33. Langer J, Hoffmann MJ, Guillon O (2009) Direct comparison between hot pressing and electric field-assisted sintering of submicron alumina. Acta Mater 57:5454–5465
34. Helle AS, Easterling KE, Ashby MF (1985) Hot-isostatic pressing diagrams: new developments. Acta Metall 33(12):2163–2174
35. Olevsky EA, Bradbury WL, Haines CD, Martin DG, Kapoor D (2012) Fundamental aspects of spark plasma sintering: I. Experimental analysis of scalability. J Am Ceram Soc 95(8):2406–2413
36. Aman Y, Garnier V, Djurado E (2011) Spark plasma sintering of pure α-alumina. J Am Ceram Soc 94(9):2825–2833
37. Frost HJ, Ashby MF (1982) Deformation-mechanism maps, the plasticity and creep of metals and ceramics. Pergamon Press, Oxford
38. Ruano OA, Wadsworth J, Sherby OD (2003) Deformation of fine-grained alumina by grain boundary sliding accommodated by slip. Acta Mater 51(12):3617–3634
39. Calvié E, Joly-Pottuz L, Esnouf C, Clément P et al (2012) Real time TEM observation of alumina ceramic nano-particles during compression. J Europ Ceram Soc 32(10):2067–2071
40. Watchman JB, Maxwell LH (1959) Strength of synthetic single crystal sapphire and ruby as a function of temperature and orientation. J Am Ceram Soc 42(9):432–433
41. Álvarez Clemares I, Borrell A, Agouram S, Torrecillas R, Fernández A (2013) Microstructure and mechanical effects of spark plasma sintering in alumina monolithic ceramics. Scr Mater 68(8):603–606
42. Morita K, Kim B-N, Yoshida H, Hiraga K (2010) Densification behavior of a fine-grained $MgAl_2O_4$ spinel during spark plasma sintering (SPS). Scr Mater 63:565–568
43. Raether F, Schulze Horn P (2009) Investigation of sintering mechanisms of alumina using kinetic field and master sintering diagrams. J Europ Ceram Soc 29(11):2225–2234
44. Brook RJ (1982) Fabrication principles for the production of ceramics with superior mechanical properties. Proc Br Ceram Soc 32:7–24
45. Heuer A (2008) Oxygen and aluminum diffusion in α-Al_2O_3: how much do we really understand? J Europ Ceram Soc 28(7):1495–1507
46. Zhou Y, Hirao K, Yamauchi Y, Kanzaki S (2004) Densification and grain growth in pulse electric current sintering of alumina. J Europ Ceram Soc 24:3465–3470